

Generation of Spatiotemporal Vortex Pulses by Resonant Diffractive Grating


Zhiyuan Che¹,¹ Wenzhe Liu^{2,*}, Junyi Ye,¹ Lei Shi^{1,3,4,†}, C. T. Chan,^{2,‡} and Jian Zi^{1,3,4,§}

¹State Key Laboratory of Surface Physics, Key Laboratory of Micro- and Nano-Photonic Structures (Ministry of Education), and Department of Physics, Fudan University, Yangpu District, Shanghai, 200433, China

²Department of Physics, The Hong Kong University of Science and Technology, Clear Water Bay, Kowloon, Hong Kong, 999077, China

³Institute for Nanoelectronic Devices and Quantum Computing, Fudan University, Yangpu District, Shanghai, 200438, China

⁴Collaborative Innovation Center of Advanced Microstructures, Nanjing University, Gulou District, Nanjing, 210093, China

 (Received 20 September 2023; accepted 3 January 2024; published 25 January 2024)

Spatiotemporal vortex pulses are wave packets that carry transverse orbital angular momentum, exhibiting exotic structured wave fronts that can twist through space and time. Existing methods to generate these pulses require complex setups like spatial light modulators or computer-optimized structures. Here, we demonstrate a new approach to generate spatiotemporal vortex pulses using just a simple diffractive grating. The key is constructing a phase vortex in frequency-momentum space by leveraging symmetry, resonance, and diffraction. Our approach is applicable to any wave system. We use a liquid surface wave (gravity wave) platform to directly demonstrate and observe the real-time generation and evolution of spatiotemporal vortex pulses. This straightforward technique provides opportunities to explore pulse dynamics and potential applications across different disciplines.

DOI: [10.1103/PhysRevLett.132.044001](https://doi.org/10.1103/PhysRevLett.132.044001)

Introduction and theory.—Spatiotemporal vortex pulses (STVPs) are structured wave packets possessing optical angular momentum transverse to their propagation direction [1–12], imparting a twisting wave front spinning like a wheel through space and time. These exotic pulses are the analogs of widely studied vortex beams [13–21]. Unlike vortex beams, which are confined to three dimensions, STVPs can exist in two dimensions, such as in surface waves. This unique property expands their potential applications beyond those possible with vortex beams alone. One promising application is spatiotemporal differentiation, enabled by the frequency-momentum space transfer function of a spatiotemporal vortex generator to perform analog pulse differentiation [22–24]. This functionality extends the concept of “topological differentiators,” first proposed for spatial image differentiation by shaping transfer functions using topological vortices in reciprocal space by Zhu *et al.* [25].

Existing STVP generation techniques typically rely on wave-front-shaping devices like spatial light modulators [5,10], or engineered metasurfaces [23,24,26–28]. Planar periodic structures, e.g., photonic crystal slabs, are ideal candidates for spatiotemporally modulating these wheel-like wave packets because they offer frequency and in-plane wave-vector degrees of freedom [29–34], the reciprocal spaces of time and position. Modulation in frequency-momentum domain directly manifests in the pulse’s space-time properties [22–24,26–28]. Introducing a phase vortex in frequency-momentum domain generates an STVP. Here, we propose a general approach to generate

STVPs using a simple diffractive grating. The key insight is harnessing symmetry, resonance, and diffraction to construct a phase vortex in frequency-momentum space that directly manifests as a twisting pulse in time and space. We experimentally demonstrate this approach and visualize generated spatiotemporal vortex pulses in real time using a liquid surface wave platform [12,35–40]. Furthermore, we show by incorporating additional resonances, our approach can generate multiple singularities within a single STVP.

Our approach has three simple prerequisites for the structures [Fig. 1(a)]. First, periodicity in one or more dimensions [x direction in our example shown in Fig. 1(a)] supporting resonant band structures. These resonances play a key role in producing the frequency-momentum domain [ω - k_x space for the grating in Fig. 1(a)] phase vortices. Second, a perfect mirror substrate blocking transmission, allowing only specular and diffractive reflection. Third, mirror symmetry about a plane [y - z plane in Fig. 1(a)] perpendicular to the periodic direction. Having these three prerequisites suffices for structures of any wave system, whether scalar or vectorial, transverse or longitudinal, electromagnetic or mechanical, to generate STVPs through our approach.

For our approach, the incident angle and frequency are chosen where only specular reflection and -1st-order diffraction are induced by the scattering of the structure [Fig. 1(b)]. In other words, the incoming waves scatter into two scattering channels. Resonances supported by the slab in this frequency-momentum region couple inputs through one channel to the other. At the X point of the Brillouin

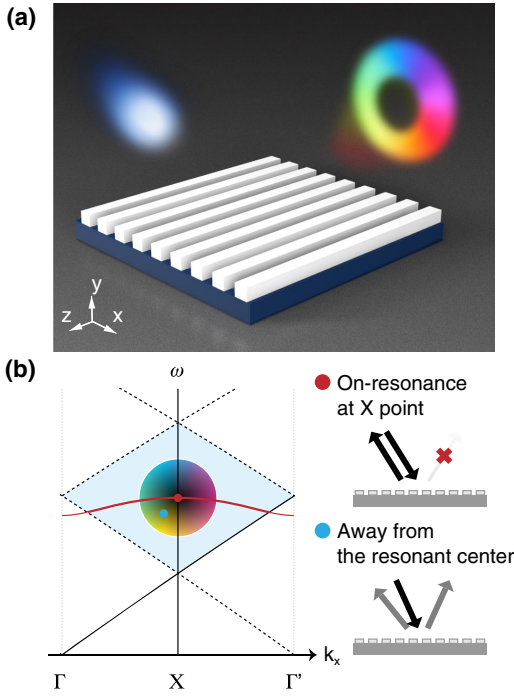


FIG. 1. Diffractive generation approach of spatiotemporal vortex pulses (STVPs) by mirror-based grating. (a) A STVP centered at a specific frequency can be generated from Gaussian pulses by a simple mirror-based resonant grating. (b) Diffraction and the mirror symmetry of the grating gives rise to this wave phenomenon. The blue-shaded region corresponds to the momentum-frequency range where the grating supports only the specular reflection and the -1st-order diffraction (i.e., two scattering channels). A phase singularity in specular reflection is formed at the X point in momentum space due to resonance-induced total retroreflection.

zone ($k_x = \pi/a$), mirror symmetry enables symmetry-protected resonant total retroreflection. The on-resonance scattering cancels the specular reflection by destructive interference, and it completely transfers energy between channels. We note that the possibility of achieving total retroreflection using diffraction gratings on perfect reflectors through symmetric and antisymmetric excitations has also been analyzed in detail in prior theoretical works [41,42]. Specular reflection vanishes at such an ω - k_x point, but is generally nonzero elsewhere [Fig. 1(b)]. This point is hence a singularity analytically predicted to have a surrounding ± 1 phase vortex [see Supplemental Material (SM) [43] for proof]. Illumination by a pulse having frequency-momentum components spanning this vortex transfers the winding phase to the pulse, yielding an STVP.

Simulation results.—Compared to past studies, our approach eliminates the need for complex setups like spatial light modulators or optimized structures. To demonstrate universality, we apply it to a liquid-surface-wave (gravity-wave) system [12,35–40]. The structure is a hard-boundary-based rectangular grating periodic in the x direction [Fig. 2(a), inset], leading to well-defined in-plane

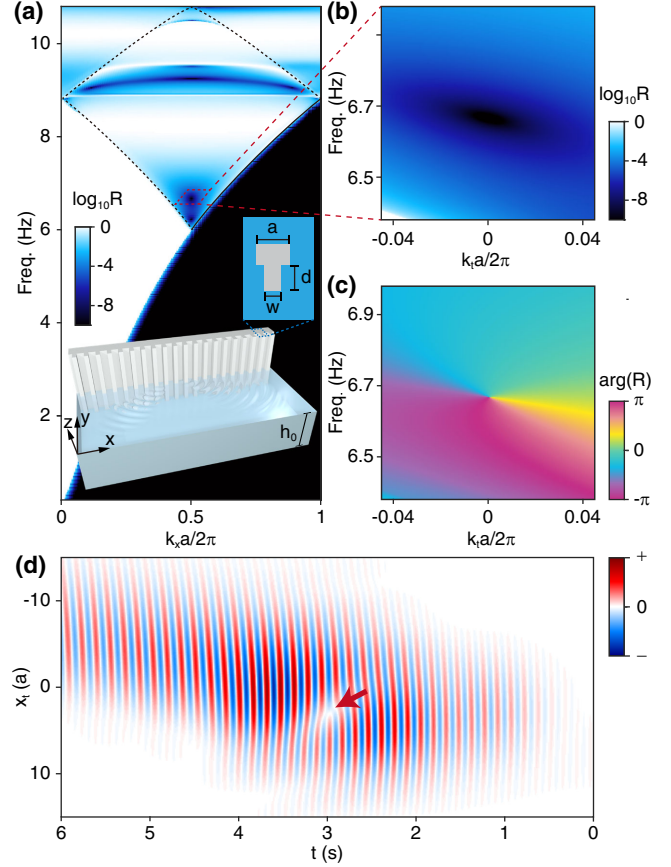


FIG. 2. Properties of the resonant mirror-based grating for STVP generation in a liquid-surface-wave system. (a) Simulated momentum-frequency reflectance map by the designed grating. The two-channel region in frequency-momentum space is enclosed by dashed curves, corresponding to the blue-shaded region in Fig. 1(b). The inset provides a schematic of the system and the grating structure. (b) Close-up of reflectance map around the singularity (with zero specular reflectance) at the X point applied to generate the STVP. The frequency of the singularity is about 6.67 Hz. (c) Corresponding reflection phase map showing a 2π phase vortex around the singularity. (d) Spatiotemporal pulse profile obtained by Fourier transforming the reflectance and phase maps with an assumed incident Gaussian pulse centered at the singularity frequency, showing an STVP.

wave vector k_x . The grating's rectangular shape provides necessary mirror symmetry to planes parallel to the y - z plane, and it enables diffraction.

Free surface wave propagation follows the dispersion relation [35]:

$$\omega^2 = (gk + \sigma k^3/\rho) \tanh(kh_0).$$

Here, ω is the angular frequency of waves, k is the free-space wave vector, g is the gravitational acceleration, σ is surface tension, ρ is liquid density, and h_0 denotes the undeformed liquid depth. This dispersion relation allows determining allowed propagation modes (the cone of radiation continuum), analogous to light cones in photonics. We consider

small amplitude (wave amplitude \ll wavelength), low frequency (6–10 Hz) waves where nonlinear and damping effects are minimal.

Introducing the hard-boundary corrugated grating [Fig. 2(a) inset] produces confined resonant guided modes and associated band structures in momentum space [29–31,38]. Grating-induced scattering also folds the radiation cones, opening diffraction channels in specific ω - k_x regions. Resonance bands naturally overlap with the region with only specular reflection and -1st-order diffraction. Within this overlap region, resonances route a portion of the power in the incident plane waves from the specular reflection channel to the diffraction channel, causing dips in the specular reflectance. At high-symmetry X point ($k_x = \pi/a$, a : grating period) and inside this ω - k_x region, total-retroreflection points induced by resonances (where all the incident power is resonantly diffracted and specular reflectance becomes zero) can be found—acting as ω - k_x domain singularities that can generate STVPs.

Figure 2(a) shows the ω - k_x -space specular reflectance map for a grating with parameters: $a = 20$ mm; grating width $w = 0.5a$; and depth $d = 1.12a$. The aforementioned two-channel region is enclosed by dashed curves, corresponding to the blue-shaded region in Fig. 1(b). Within this region, specular reflectance dips indicate resonances.

As discussed, there are several frequencies at the X point where the specular reflectance approaches zero, corresponding to total retroreflection points. The specular reflectance map has been logarithmically scaled to highlight these points. Figure 2(b) focuses in on a total retroreflection point at $f_0 = 6.67$ Hz. This is the singularity we will utilize for STVP generation. Accordingly, Fig. 2(c) reveals an enclosing 2π phase vortex, as predicted. Note that in Figs. 2(b) and 2(c), the horizontal axis is k_t rather than the in-plane wave vector k_x . k_t is the transverse component of the reflected wave vector with respect to a center propagation wave vector $\mathbf{k}(\omega_0)$, obtained by the transform $k_t = k \sin\{\arcsin(k_x/k) - \arcsin[\pi/a/k(\omega_0)]\}$ where ω_0 is the singularity's angular frequency.

The specularly reflected pulse profile modulated by the grating can be predicted by Fourier transforming the reflectance and phase maps in Figs. 2(a)–2(c), assuming an incident Gaussian pulse centered at the singularity frequency ω_0 . (Details are provided in SM [43]). Figure 2(d) shows the resulting predicted STVP, with a fork-shaped pattern (red arrow) signifying the presence of a 2π vortex in the space-time domain, corresponding to the phase vortex observed in Fig. 2(c). The STVP vortex stems from the phase singularity at the total retroreflection point in the ω - k_x maps.

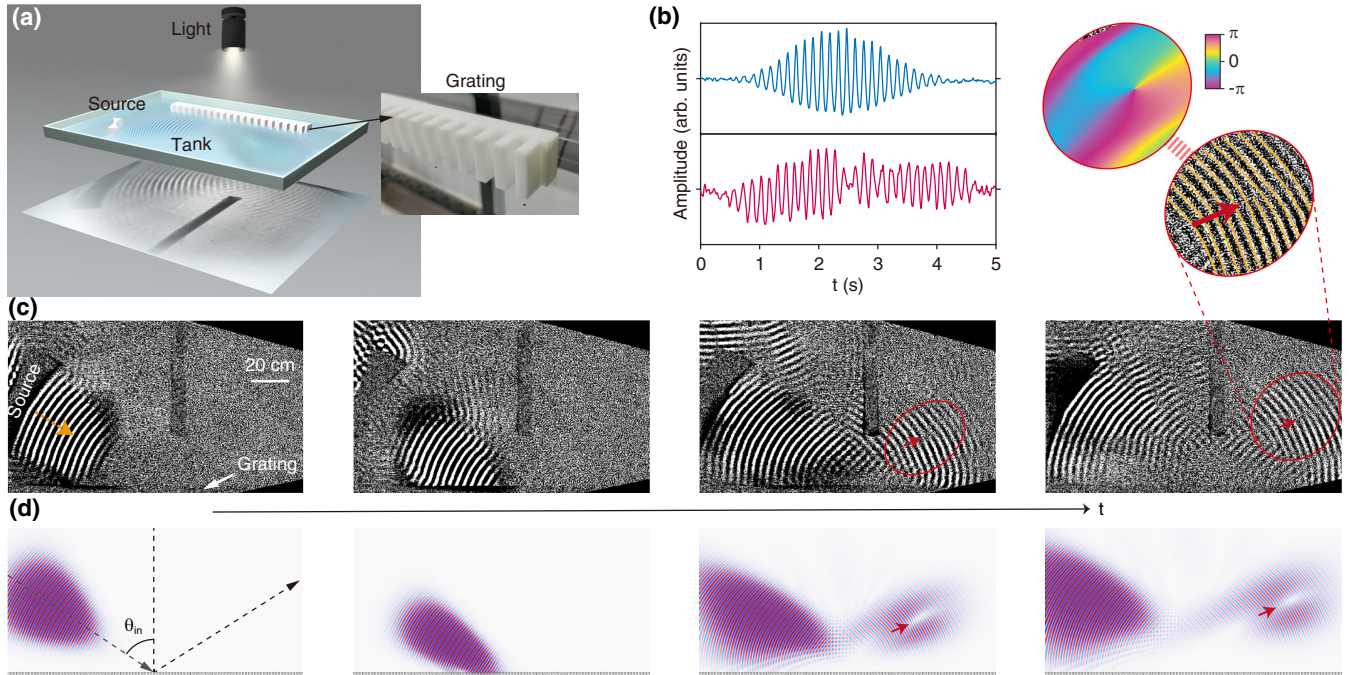


FIG. 3. Experimental demonstration of STVP generation using a resonant mirror-based grating. (a) Schematic of the experimental setup. The grating is placed in a transparent tank containing $C_2H_3ClF_2$ (1-chloro-1,1-difluoroethane) liquid with a depth of $h_0 \sim 1.1$ cm. A concave-shaped source is driven by a computer-controlled speaker to emit the incident Gaussian pulse. Inset: photograph of the 3D-printed grating. (b) Measured time signals of the incident Gaussian pulse and reflected STVP, and Fourier-transformed spectra showing normalized spectral intensity of pulses. The signals are sampled at points where the centers of pulses pass. (c) Sequence of time-resolved images showing the reflection process and propagation of the reflected STVP. A retro-reflecting pulse can be observed on the left, while the STVP is in the specular reflecting direction on the right. (d) Simulated time sequence of images for comparison. The central angle of incident pulse, θ_{in} , is about 57.3° .

Experimental demonstration and discussion.—We experimentally observed STVP generation using a projected wave tank system, shown in Fig. 3(a). The system has a transparent tank filled with 1-chloro-1,1-difluoroethane ($C_2H_3ClF_2$) liquid (surface tension $\sim 1/4$ water's, for lower damping) to a depth of $h_0 \sim 1.1$ cm. A light above the tank projects the wave pattern onto a plane beneath, which can be directly observed or captured on video for analysis. The 3D-printed grating we designed is placed inside the tank [see photograph in Fig. 3(a)]. A computer-controlled concave speaker source emits Gaussian pulses, with the curvature intentionally designed to shape the wave fronts into spatially Gaussian at the grating plane. The time signals of the incident Gaussian pulses are sampled at points where the pulse centers pass, as shown by the blue curve in Fig. 3(b).

Figure 3(c) shows the time-resolved image sequence of the reflection process and STVP propagation. In the first image (left), a Gaussian pulse (~ 2 s, bandwidth ~ 0.64 Hz, central frequency 7.02 Hz) is emitted and propagates toward the grating (at the bottom). The incident pulse then impinges on the grating (second image). The third and fourth images show the reflected pulse, and we see that the STVP has been generated and propagates on the specular side, marked by a red ellipse. A fork-shaped pattern (marked by red arrows), similar to that in Fig. 2(d), is highlighted by yellow lines. By Fourier transforming the image and filtering out the central spatial frequency, we extract the pulse phase distribution, which exhibits a phase vortex [Fig. 3(c) inset]. Note that the waves on the left in the last two images are intended retroreflected waves. Stray waves are also present caused by the finite emitter size. These waves reflect off and interfere, producing unintended interference patterns and noisy singularities. However, the key features of the generated STVP remain identifiable on the right. The Video in Supplemental Material shows the complete process [43]. For reference, Fig. 3(d) presents the simulated time sequence. Simulations agree well with experiments. We also extracted the reflected wave time signal at the STVP center [Fig. 3(b), red curve]. Compared to the incident time signal, an obvious π phase jump is visible, corresponding to the frequency domain singularity. Overall, the experiments are consistent with theoretical expectations.

With single STVP generation demonstrated, we next explore creating multiple singularities within a single spatiotemporal pulse. As emphasized above, our STVP generation approach requires only symmetry, resonance, and diffraction. This enables engineering multiple ω - k_x domain vortices without changing grating symmetry or diffraction orders, and we can generate pulses with multiple spatiotemporal singularities by tuning grating depth and filling fraction. We achieve diverse ω - k_x -domain vortex configurations owing to resonance tunability.

Figure 4(a) shows simulated specular reflectance spectra at the X point as a function of grating depth d , with other

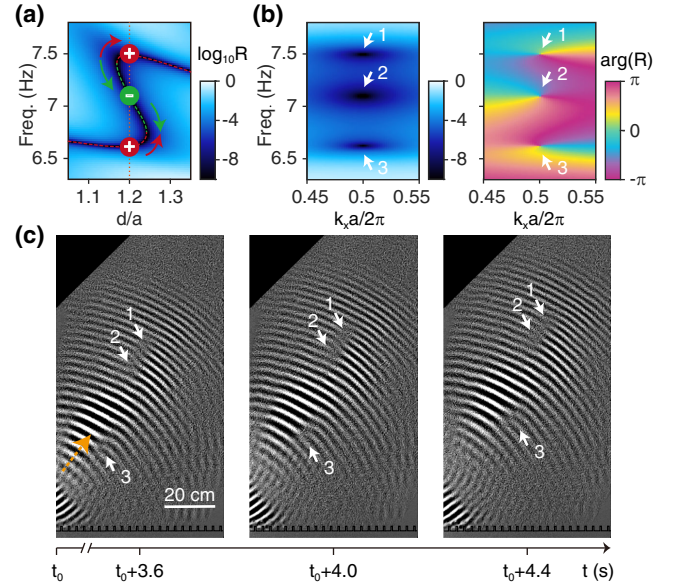


FIG. 4. Evolution of phase vortices in the parameter space and coexistence of multiple singularities in one pulse. (a) Simulated reflectance spectrum at the X point as a function of the grating depth d . As d increases, a singularity with $+1$ topological charge evolves into three charges (one $+1$ charge and a pair of ± 1 charges). Upon a further increase of d , the $+1$ charge annihilates with the -1 charge, leaving the other $+1$ charge. The total topological charge is conserved. (b) Momentum-frequency reflectance map for $d = 1.2a$ (marked by orange dashed line in (a)). The corresponding reflection phase exhibits two phase vortices with $+1$ charges and one with a -1 charge. (c) Experimentally measured space-time evolution of a chirped pulse with multiple singularities reflected from the grating for $d = 1.2a$. A two-second Gaussian pulse with negative linear frequency chirp spanning 3.78 sec is emitted from the source. Three images show the reflected pulse containing three fork dislocations matching the designed ω - k_x space vortices.

parameters fixed ($a = 30$ mm; $w = 0.2a$). As d increases, we observe the complete evolution of total retroreflection points (singularities in ω - k_x domain) in the parameter space, including their generation and annihilation. Initially, for $d < 1.16a$, there is a single $+1$ singularity at ~ 6.6 Hz. At $d \sim 1.16a$, a pair of oppositely charged singularities appear near 7.45 Hz. With d further increasing, the -1 singularity approaches the original $+1$ singularity. At $d \sim 1.24a$, the -1 singularity eventually annihilates original $+1$ singularity at ~ 6.67 Hz, leaving only the $+1$ singularity at ~ 7.46 Hz. For $d > 1.24a$, there is again only one $+1$ singularity. The total topological charge is conserved throughout this process.

As a concrete example, Fig. 4(b) depicts the ω - k_x -domain specular reflection phase map for $d = 1.2a$ [dashed line in Fig. 4(a)]. Three total-retroreflection points are present, revealing two $+1$ -charged phase vortices at ~ 6.7 Hz and ~ 7.57 Hz and one -1 vortex at ~ 7.2 Hz. The vortex coexistence enables observing the real-time generation and evolution of a STVP with multiple singularities.

In real space-time, the ω - k_x domain singularities manifest as phase vortices. Figure 4(c) shows the space-time evolution of a chirped pulse reflected from the grating with three singularities for $d = 1.2a$. A Gaussian pulse (bandwidth ~ 0.64 Hz, central frequency 7.25 Hz) with original duration of 2 sec [whose frequency-momentum bandwidth covers all the three singularities in Fig. 4(b)] and a negative linear frequency chirp (chirped duration 3.78 s) is emitted from the source, with higher frequencies in the front and lower frequencies behind.

The images in Fig. 4(c) show the propagation of the reflected pulse at different times. The time when the center of the incident pulse coincides with the grating is denoted as t_0 . In the first image at $t_0 + 3.6$ s, three fork patterns have emerged. The fork dislocation in the front of the pulse corresponds to the $+1$ vortex designed at 7.57 Hz, associated with the higher frequencies at the start of the chirped pulse. Behind it, the central fork pattern corresponds to the -1 vortex at 7.2 Hz. At the back, the third fork corresponds to the $+1$ vortex at 6.7 Hz. The subsequent images at $t_0 + 4.0$ s and $t_0 + 4.4$ s show the propagation of the pulse. The forks' positions matching the frequency sweep validates the designed mapping between frequency-momentum and real space-time. The ability to produce pulses with multiple singularities highlights the versatility of our general diffractive approach.

Conclusions.—In summary, we have introduced a general diffractive approach to generate spatiotemporal vortex pulses in diverse wave systems using resonant planar periodic structures. By harnessing universal wave phenomena of symmetry, diffraction, and resonance, phase vortices can be achieved in frequency-momentum domain without complex designs. Through the natural reciprocal relationship, this controlled modulation in frequency-momentum domain manifests directly as structured STVP wave forms. We demonstrated the approach with liquid surface (gravity) waves, which is the first demonstration of “water-wave” STVPs proposed by Smirnova *et al.* [12]. This establishes a versatile framework for wave-front manipulation with potential innovations across disciplines. Further efforts are still needed to fully investigate emerging opportunities, and our approach expands the toolkit for investigating novel spatiotemporal degrees of freedom. Looking forward, we hope this work encourages multi-disciplinary pursuits of fundamental questions and applications related to spatiotemporally-structured pulses [44–47], angular momenta [48,49], and singularities [50–52] in waves.

The authors acknowledge the support of National Key Research and Development Program of China (2022YFA1404800, 2021YFA1400603); National Natural Science Foundation of China (No. 12234007 and No. 12221004); Major Program of National Natural Science Foundation of China (No. 91963212); Science and Technology Commission of Shanghai Municipality

(22142200400, 21DZ1101500, 2019SHZDZX01); China Postdoctoral Science Foundation (2022M720810, 2022TQ0078). This work is also supported by the Research Grants Council of Hong Kong through Grants No. AoE/P-502/20 and No. A-HKUST601/18, and the Croucher Foundation (CAS20SC01).

All the authors discussed, interpreted the results, and conceived the theoretical framework. W.L. and J.Z. conceived the basic idea of the work. Z.C. extended the model to liquid surface waves and designed the simulations. Z.C., W.L., and L.S. designed the experiments. Z.C. performed the experiments. J.Y. and Z.C. analyzed the experimental data. L.S., C.T.C., and J.Z. supervised the research and the development of the manuscript. Z.C., W.L., L.S., and C.T.C. wrote the manuscript draft. All authors took part in the discussion, revision, and approved the final copy of the manuscript. Z.C. and W.L. contributed equally to this work.

*wliubh@connect.ust.hk

†lshi@fudan.edu.cn

‡phchan@ust.hk

§jzi@fudan.edu.cn

- [1] N. Dror and B. A. Malomed, Symmetric and asymmetric solitons and vortices in linearly coupled two-dimensional waveguides with the cubic-quintic nonlinearity, *Physica (Amsterdam)* **240D**, 526 (2011).
- [2] K. Y. Bliokh and F. Nori, Spatiotemporal vortex beams and angular momentum, *Phys. Rev. A* **86**, 033824 (2012).
- [3] N. Jhajj, I. Larkin, E. W. Rosenthal, S. Zahedpour, J. K. Wahlstrand, and H. M. Milchberg, Spatiotemporal optical vortices, *Phys. Rev. X* **6**, 031037 (2016).
- [4] S. W. Hancock, S. Zahedpour, A. Goffin, and H. M. Milchberg, Free-space propagation of spatiotemporal optical vortices, *Optica* **6**, 1547 (2019).
- [5] A. Chong, C. Wan, J. Chen, and Q. Zhan, Generation of spatiotemporal optical vortices with controllable transverse orbital angular momentum, *Nat. Photonics* **14**, 350 (2020).
- [6] K. Y. Bliokh, Spatiotemporal vortex pulses: Angular momenta and spin-orbit interaction, *Phys. Rev. Lett.* **126**, 243601 (2021).
- [7] S. W. Hancock, S. Zahedpour, and H. M. Milchberg, Mode structure and orbital angular momentum of spatiotemporal optical vortex pulses, *Phys. Rev. Lett.* **127**, 193901 (2021).
- [8] Q. Cao, J. Chen, K. Lu, C. Wan, A. Chong, and Q. Zhan, Non-spreading Bessel spatiotemporal optical vortices, *Sci. Bull.* **67**, 133 (2022).
- [9] K. Y. Bliokh, Orbital angular momentum of optical, acoustic, and quantum-mechanical spatiotemporal vortex pulses, *Phys. Rev. A* **107**, L031501 (2023).
- [10] H. Ge, S. Liu, X.-Y. Xu, Z.-W. Long, Y. Tian, X.-P. Liu, M.-H. Lu, and Y.-F. Chen, Spatiotemporal acoustic vortex beams with transverse orbital angular momentum, *Phys. Rev. Lett.* **131**, 014001 (2023).

- [11] M. A. Porras, Transverse orbital angular momentum of spatiotemporal optical vortices, *Prog. Electromagn. Res.* **177**, 95 (2023).
- [12] D. A. Smirnova, F. Nori, and K. Y. Bliokh, Water-wave vortices and skyrmions, [arXiv:2308.03520](https://arxiv.org/abs/2308.03520) [Phys. Rev. Lett. (to be published)].
- [13] L. Allen, M. W. Beijersbergen, R. J. C. Spreeuw, and J. P. Woerdman, Orbital angular momentum of light and the transformation of Laguerre-Gaussian laser modes, *Phys. Rev. A* **45**, 8185 (1992).
- [14] K. Y. Bliokh, Geometrical optics of beams with vortices: berry phase and orbital angular momentum hall effect, *Phys. Rev. Lett.* **97**, 043901 (2006).
- [15] M. R. Dennis, K. O'Holleran, and M. J. Padgett, in *Progress in Optics* (Elsevier, New York, 2009), Vol. 53, pp. 293–363.
- [16] S. Chen, Y. Cai, G. Li, S. Zhang, and K. W. Cheah, Geometric metasurface fork gratings for vortex-beam generation and manipulation, *Laser Photonics Rev.* **10**, 322 (2016).
- [17] C. Huang, C. Zhang, S. Xiao, Y. Wang, Y. Fan, Y. Liu, N. Zhang, G. Qu, H. Ji, J. Han, L. Ge, Y. Kivshar, and Q. Song, Ultrafast control of vortex microlasers, *Science* **367**, 1018 (2020).
- [18] Y. Yang and C.-W. Qiu, Generation of optical vortex beams, in *Electromagnetic Vortices* (John Wiley & Sons, Ltd, New York, 2021), Chap. 7, pp. 223–244.
- [19] J. Ni, C. Huang, L.-M. Zhou, M. Gu, Q. Song, Y. Kivshar, and C.-W. Qiu, Multidimensional phase singularities in nanophotonics, *Science* **374**, eabj0039 (2021).
- [20] X. Zhang, L. Huang, R. Zhao, Q. Wei, X. Li, G. Geng, J. Li, X. Li, Y. Wang, and S. Zhang, Multiplexed generation of generalized vortex beams with On-Demand intensity profiles based on metasurfaces, *Laser Photonics Rev.* **16**, 2100451 (2021).
- [21] H. Wang, H. Wang, Q. Ruan, J. Y. E. Chan, W. Zhang, H. Liu, S. D. Rezaei, J. Trisno, C.-W. Qiu, M. Gu, and J. K. W. Yang, Coloured vortex beams with incoherent white light illumination, *Nat. Nanotechnol.* **18**, 264 (2023).
- [22] L. L. Doskolovich, A. I. Kashapov, E. A. Bezus, and D. A. Bykov, Spatiotemporal optical differentiation and vortex generation with metal-dielectric-metal multilayers, *Phys. Rev. A* **106**, 033523 (2022).
- [23] J. Huang, J. Zhang, T. Zhu, and Z. Ruan, Spatiotemporal differentiators generating optical vortices with transverse orbital angular momentum and detecting sharp change of pulse envelope, *Laser Photonics Rev.* **16**, 2100357 (2022).
- [24] Y. Zhou, J. Zhan, Z. Xu, Y. Shao, Y. Wang, Y. Dang, S. Zhang, and M. Yungui, Electromagnetic spatiotemporal differentiators, [arXiv:2308.03797](https://arxiv.org/abs/2308.03797).
- [25] T. Zhu, C. Guo, J. Huang, H. Wang, M. Orenstein, Z. Ruan, and S. Fan, Topological optical differentiator, *Nat. Commun.* **12**, 680 (2021).
- [26] H. Wang, C. Guo, W. Jin, A. Y. Song, and S. Fan, Engineering arbitrarily oriented spatiotemporal optical vortices using transmission nodal lines, *Optica* **8**, 966 (2021).
- [27] A. I. Kashapov, E. A. Bezus, D. A. Bykov, and L. L. Doskolovich, Plasmonic generation of spatiotemporal optical vortices, *Photonics* **10**, 109 (2023).
- [28] H. Zhang, Y. Sun, J. Huang, B. Wu, Z. Yang, K. Y. Bliokh, and Z. Ruan, Topologically crafted spatiotemporal vortices in acoustics, *Nat. Commun.* **14**, 6238 (2023).
- [29] S. G. Johnson, S. Fan, P. R. Villeneuve, J. D. Joannopoulos, and L. A. Kolodziejski, Guided modes in photonic crystal slabs, *Phys. Rev. B* **60**, 5751 (1999).
- [30] S. Fan and J. D. Joannopoulos, Analysis of guided resonances in photonic crystal slabs, *Phys. Rev. B* **65**, 235112 (2002).
- [31] S. Fan, W. Suh, and J. D. Joannopoulos, Temporal coupled-mode theory for the Fano resonance in optical resonators, *J. Opt. Soc. Am. A* **20**, 569 (2003).
- [32] C. Guo, H. Wang, and S. Fan, Squeeze free space with nonlocal flat optics, *Optica* **7**, 1133 (2020).
- [33] B. Wang, W. Liu, M. Zhao, J. Wang, Y. Zhang, A. Chen, F. Guan, X. Liu, L. Shi, and J. Zi, Generating optical vortex beams by momentum-space polarization vortices centred at bound states in the continuum, *Nat. Photonics* **14**, 623 (2020).
- [34] J. Wang, M. Zhao, W. Liu, F. Guan, X. Liu, L. Shi, C. T. Chan, and J. Zi, Shifting beams at normal incidence via controlling momentum-space geometric phases, *Nat. Commun.* **12**, 6046 (2021).
- [35] M. W. Dingemans, *Water Wave Propagation over Uneven Bottoms* (World Scientific Publishing Company, Singapore, 1997), Vol. 13.
- [36] X. Hu and C. T. Chan, Refraction of water waves by periodic cylinder arrays, *Phys. Rev. Lett.* **95**, 154501 (2005).
- [37] X. Zhao, X. Hu, and J. Zi, Fast water waves in stationary surface disk arrays, *Phys. Rev. Lett.* **127**, 254501 (2021).
- [38] L. Han, S. Chen, and H. Chen, Water wave polaritons, *Phys. Rev. Lett.* **128**, 204501 (2022).
- [39] Z. Qin, C. Qian, L. Shen, X. Wang, I. Kaminer, H. Chen, and H. Wang, Superscattering of water waves, *Natl. Sci. Rev.* **10**, nwac255 (2022).
- [40] J. Zeng, X. Zhao, X. Sun, and X. Hu, Achieving complete band gaps of water waves with shallow-draft cylinder arrays, *Phys. Rev. Appl.* **19**, 044058 (2023).
- [41] H. Wei and L. Li, All-dielectric reflection gratings: a study of the physical mechanism for achieving high efficiency, *Appl. Opt.* **42**, 6255 (2003).
- [42] L. Li, Internal mechanism of perfect-reflector-backed dielectric gratings to achieve high diffraction efficiency, *EPJ Web Conf.* **287**, 04022 (2023).
- [43] See Supplemental Material at <http://link.aps.org/supplemental/10.1103/PhysRevLett.132.044001> for notes and figures about (1) numerical calculations for liquid surface waves, (2) experimental setup details, (3) detailed discussion on the theory for spatiotemporal vortex pulse generation (STVP) by resonant diffractive grating, (4) supplemental simulations, (5) descriptions of supplemental videos.
- [44] A. Zdagkas, V. Nalla, N. Papisimakis, and N. I. Zheludev, Spatio-temporal characterization of ultrashort vector pulses, *APL Photonics* **6**, 116103 (2021).
- [45] C. Wan, Q. Cao, J. Chen, A. Chong, and Q. Zhan, Toroidal vortices of light, *Nat. Photonics* **16**, 519 (2022).
- [46] A. Zdagkas, C. McDonnell, J. Deng, Y. Shen, G. Li, T. Ellenbogen, N. Papisimakis, and N. I. Zheludev, Observation of toroidal pulses of light, *Nat. Photonics* **16**, 523 (2022).

- [47] Y. Shen *et al.*, Roadmap on spatiotemporal light fields, *J. Opt.* **25**, 093001 (2023).
- [48] K. Y. Bliokh and F. Nori, Spin and orbital angular momenta of acoustic beams, *Phys. Rev. B* **99**, 174310 (2019).
- [49] C. Shi, R. Zhao, Y. Long, S. Yang, Y. Wang, H. Chen, J. Ren, and X. Zhang, Observation of acoustic spin, *Natl. Sci. Rev.* **6**, 707 (2019).
- [50] H. Ge, X.-Y. Xu, L. Liu, R. Xu, Z.-K. Lin, S.-Y. Yu, M. Bao, J.-H. Jiang, M.-H. Lu, and Y.-F. Chen, Observation of acoustic skyrmions, *Phys. Rev. Lett.* **127**, 144502 (2021).
- [51] K. Y. Bliokh, M. A. Alonso, D. Sugic, M. Perrin, F. Nori, and E. Brasselet, Polarization singularities and mobius strips in sound and water-surface waves, *Phys. Fluids* **33**, 077122 (2021).
- [52] R. D. Muelas-Hurtado, K. Volke-Sepúlveda, J. L. Ealo, F. Nori, M. A. Alonso, K. Y. Bliokh, and E. Brasselet, Observation of polarization singularities and topological textures in sound waves, *Phys. Rev. Lett.* **129**, 204301 (2022).